Driven, autoresonant three-oscillator interactions

O. Yaakobi,[1,2] L. Friedland,[2,*] and Z. Henis[1]
[1]*Soreq NRC, Yavne 81800, Israel*
[2]*Racah Institute of Physics, Hebrew University, Jerusalem 91904, Israel*
(Received 3 April 2007; published 7 August 2007)

An efficient control scheme of resonant three-oscillator interactions using an external chirped frequency drive is suggested. The approach is based on formation of a double phase-locked (autoresonant) state in the system, as the driving oscillation passes linear resonance with one of the interacting oscillators. When doubly phase locked, the amplitudes of the oscillators increase with time in proportion to the driving frequency deviation from the linear resonance. The stability of this phase-locked state and the effects of dissipation and of the initial three-oscillator frequency mismatch on the autoresonance are analyzed. The associated autoresonance threshold phenomenon in the driving amplitude is also discussed. In contrast to other nonlinear systems, driven, autoresonant three-oscillator excitations are independent of the sign of the driving frequency chirp rate.

DOI: 10.1103/PhysRevE.76.026205 PACS number(s): 05.45.Xt, 52.35.Mw

I. INTRODUCTION

Resonant three-wave interactions (R3WIs) and their dynamical counterparts, three-oscillator interactions (R3OIs) play a fundamental role in physics because they represent lowest-order (in terms of wave amplitudes) nonlinear effects in systems approximately described by a linear superposition of discrete waves and oscillations [1]. For example, an incoming laser beam in a plasma can decay via R3WIs into another electromagnetic wave and an ion-acoustic or plasma wave [2]. R3WIs are also characteristic of many other fields of nonlinear physics, such as nonlinear optics [3], hydrodynamics [4], and acoustics [5]. Consequently, controlling R3WIs and R3OIs is an important goal of both basic and applied physics research. Varying the three-wave resonance condition by time and/or space inhomogeneity of the background medium is one approach to affecting R3WIs [6]. An alternative is to influence the resonance condition by nonlinearity of the medium [7]. By combining the space and time variation and the nonlinearity of the background one may use autoresonance for controlling R3WIs [8–10]. This more recent approach uses the intrinsic property of many nonlinear waves and oscillations to stay in resonance (to phase lock) even when parameters of the system vary in time and/or space [11]. In the case of three coupled waves or oscillations, the phase locking is achieved as the nonlinear frequency or wave vector shifts self-adjust (via variation of the wave amplitudes) to compensate the linear dispersion shifts due to the inhomogeneity of the background.

In this work, we shall consider a different autoresonant R3WI scheme which does not require variation of the parameters of the medium and nonlinear dispersion of the interacting waves. Thus, we shall assume that the medium is uniform and time independent and that the only nonlinearity in the problem is due to the usual three-wave resonant coupling, but introduce an additional element in the system, i.e., an external chirped frequency perturbation (drive). It is the nonlinear wave coupling combined with the slow variation of the driving frequency, that will lead to an unconventional type of autoresonance in the system. Its manifestation will be seen as the amplification of the wave amplitudes controlled by a single parameter (chirped frequency of the driving oscillation). For simplicity, instead of waves, we shall consider a system of nonlinearly coupled linear oscillators x_j $(j=1,2,3)$ governed by

$$\ddot{x}_j + \omega_j^2 x_j = -\varepsilon x_k x_3, \quad j,k=1,2, \quad j \neq k, \tag{1}$$

$$\ddot{x}_3 + \omega_3^2 x_3 = -\varepsilon x_1 x_2 - F_d. \tag{2}$$

Here we assumed the frequency-matching condition $\omega_1+\omega_2=\omega_3$, while $F_d=\eta\cos\psi_d$, where $\psi_d=\int\omega_d(t)dt$ represents a constant amplitude, chirped frequency driving perturbation in the equation for the third (driven) oscillator. All dependent and independent variables in this model system are dimensionless, such that x_j are rescaled by the initial amplitude A_{10} of the first oscillator, and the frequencies (and time) are rescaled by the linear frequency (and inverse frequency) of the first oscillator. Similarly, the dimensionless coupling coefficient ε and driving amplitude η correspond to the original $A_{10}\varepsilon/\omega_1^2$ and $\eta/(A_{10}\omega_1^2)$, respectively. Note that, for $\eta=0$, Eqs. (1) and (2) describe, for example, the well-known parametric oscillator problem [3]. Reduction (not considered in this work) of a similar system of governing equations for R3WIs would require the wave vector matching condition $\mathbf{k}_1+\mathbf{k}_2=\mathbf{k}_3$ and replacement of F_d by a chirped frequency driving wave $\eta\cos[\mathbf{k}_3\cdot\mathbf{r}-\int\omega_d(t)dt]$, but this problem is outside the scope of the present work.

We illustrate autoresonance phenomenon in our driven system in Fig. 1(a), showing the total energy $H=\Sigma_{j=1}^{3}(\dot{x}_j^2+x_j^2)/2+\varepsilon x_1x_2x_3+F_dx_3$ versus rescaled (slow) time $\tau=\sqrt{\alpha}t$, found by solving Eqs. (1) and (2) numerically for a linear (in time) driving frequency chirp $\omega_d=\omega_3+\alpha t$ (note that the drive passes the linear resonance $\omega_d=\omega_3$ at $t=0$), subject to initial conditions (at $\tau=-125$) $x_1=1$, $x_{2,3}=0$, $\dot{x}_{1,2,3}=0$. We used parameters $\omega_1=1$, $\omega_2=2$, $\omega_3=3$, $\alpha=10^{-5}$, $\varepsilon=0.031$, and $\eta=0.0174$ (solid line) in these simulations. Unless stated otherwise, these parameters will be used in all subsequent nu-

*lazar@vms.huji.ac.il

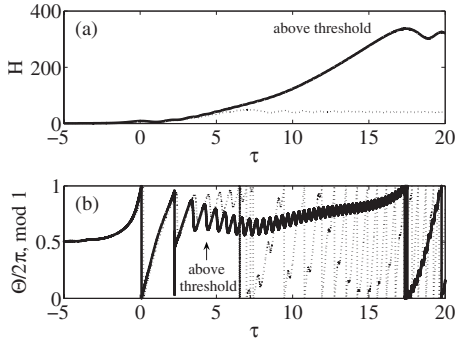

FIG. 1. Autoresonant evolution in the driven three-oscillator system. (a) Energy H and (b) phase mismatch Θ in the system just above (solid lines, $\eta=0.0174$) and below (dotted lines, $\eta=0.0155$) the threshold for autoresonance.

merical examples in this paper. All simulations in Fig. 1 and throughout this work used the Runge-Kutta, self-varying step size differential equation solver ODE45 in the standard MATLAB 7 package [12] with the assigned relative and absolute error tolerances of 10^{-9}. The decrease of the tolerances by a factor of 10 yielded no visible variation in Fig. 1. One can see in the figure a significant growth of energy H of the system with time beyond the linear resonance despite the smallness of the driving amplitude, until saturation at $\tau=17.3$. This energy amplification is accompanied by a continuing double self-phase-locking $\Theta\equiv\psi_d-\psi_3\approx$const [see Fig. 1(b)] and $\Phi\equiv\psi_3-\psi_1-\psi_2\approx 0$ in the system (not shown in the figure), where ψ_j are individual phases of the oscillators. The latter are defined by writing $x_j=\mathrm{Re}\{A_j(t)\exp[-i\psi_j(t)]\}, \mathrm{Im}(A_j,\psi_j)=0$ and found numerically by forming the analytic signal using the Hilbert transform of x_j [13]. Figure 1 also illustrates another important characteristic of autoresonance in our system, i.e., the existence of a threshold in the driving amplitude for capture into autoresonance. Indeed, the dotted lines in the figure represent simulations with all parameters the same, but $\eta=0.0155$ (the threshold value in this case is $\eta_{th}=0.0167$). One can see that the phase-locking $\Theta\equiv\psi_d-\psi_3\approx$const discontinues in this case not far beyond the linear resonance, resulting in energy saturation at a relatively small value. We found that autoresonance in this system is achieved independently of the sign of the driving frequency chirp rate. This is substantially different from the usual autoresonance of nonlinear oscillations, where the sign of the frequency chirp rate must correspond to the sign of the weakly nonlinear frequency shift for successful excitation [14].

The understanding of the details of the autoresonant interaction in our driven system, as illustrated in Fig. 1, is the main goal of the present work. The scope of the paper will be as follows. The capture of the system into resonance and the resulting autoresonant quasi-steady-state will be discussed in Sec. II. Section III will deal with the problem of stability of the quasi-steady-state. We shall discuss the autoresonance threshold phenomenon in driven R3OI systems in Sec. IV. The validity of the small nonlinear frequency shift model will be considered in Sec. V. Finally, in Secs. V and VI, we shall include the effects of dissipation and linear frequency mismatch on the autoresonance and present our conclusions.

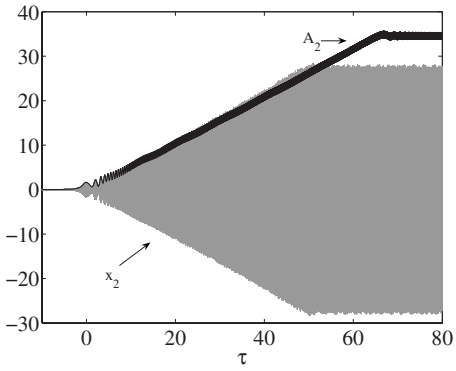

FIG. 2. Comparison between the solution of the original equations (1) and (2) for x_2 and the adiabatic approximation, Eqs. (3)–(7), for slow envelope A_2, using parameters $\varepsilon=0.031$ and $\eta=0.0197$.

II. AUTORESONANT EVOLUTION

A. Adiabatic approximation

We precede our analysis of the autoresonance in the driven system by introducing the usual adiabatic representation $x_j=\mathrm{Re}(A_j e^{-i\psi_j})$, $j=1,2,3$, where A_j and the phases ψ_j are real functions of time. We shall assume that the amplitudes A_j are slow on the scale of periods of the linear oscillations. In contrast, the phases ψ_j are fast, but the two phase mismatches $\Phi\equiv\psi_3-\psi_1-\psi_2$ and $\Theta\equiv\psi_d-\psi_3$ are assumed to be slow. Then, by substituting x_j into Eqs. (1) and (2), neglecting $\ddot{A}_j$, keeping the resonant terms only, and separating the real and imaginary parts, we obtain the following set of slow evolution equations:

$$\dot{A}_j\Omega_j+\frac{1}{2}A_j\dot{\Omega}_j=-\frac{\varepsilon}{4}A_kA_3\sin\Phi,\quad j,k=1,2,\quad j\neq k, \tag{3}$$

$$\dot{A}_3\Omega_3+\frac{1}{2}A_3\dot{\Omega}_3=\frac{\varepsilon}{4}A_1A_2\sin\Phi-\frac{\eta}{2}\sin\Theta, \tag{4}$$

$$\Omega_j^2=\omega_j^2+\frac{\varepsilon}{2}\frac{A_kA_3}{A_j}\cos\Phi,\quad j,k=1,2,\quad j\neq k, \tag{5}$$

$$\Omega_3^2=\omega_3^2+\frac{\varepsilon}{2}\frac{A_1A_2}{A_3}\cos\Phi+\frac{\eta}{A_3}\cos\Theta, \tag{6}$$

$$\dot{\Phi}=\Omega_3-\Omega_1-\Omega_2,\quad \dot{\Theta}=\omega_3+\alpha t-\Omega_3, \tag{7}$$

where $\Omega_j=\dot{\psi}_j$. Throughout this work, we consider evolution of our three-oscillator system, subject to finite initial amplitude of the first oscillator (the pump), $A_{10}=1$, and vanishing initial amplitudes $A_{20,30}=0$ of the second and third oscillators. We compare numerical solutions of the original set of equations (1) and (2) versus $\tau=\sqrt{\alpha}t$ with those of our adiabatic approximation [Eqs. (3)–(7)] in Fig. 2, using parameters $\varepsilon=0.031$ and $\eta=0.0197$ (above the threshold for autoresonance) and the same initial conditions as in Fig. 1. One can see in the figure that A_2 follows closely the envelope of

x_2, indicating that the adiabatic approximation is valid in this case.

The rescaled time τ used in Figs. 1 and 2 is the convenient independent variable in the adiabatic approximation. Consequently, prior to further analysis, we rewrite our adiabatic system as

$$\frac{dB_j}{d\tau} = -\frac{\varepsilon}{4\sqrt{\alpha\Omega_1\Omega_2\Omega_3}} B_k B_3 \sin\Phi, \quad j,k=1,2, \quad j\neq k, \tag{8}$$

$$\frac{dB_3}{d\tau} = \frac{\varepsilon}{4\sqrt{\alpha\Omega_1\Omega_2\Omega_3}} B_1 B_2 \sin\Phi - \frac{\eta}{2\sqrt{\alpha\Omega_3}} \sin\Theta, \tag{9}$$

$$\Omega_j^2 = \omega_j^2 + \frac{\varepsilon}{2}\frac{B_k B_3}{B_j}\sqrt{\frac{\Omega_j}{\Omega_k\Omega_3}}\cos\Phi, \quad j,k=1,2, \quad j\neq k, \tag{10}$$

$$\Omega_3^2 = \omega_3^2 + \frac{\varepsilon}{2}\frac{B_1 B_2}{B_3}\sqrt{\frac{\Omega_3}{\Omega_1\Omega_2}}\cos\Phi + \frac{\eta}{B_3}\sqrt{\Omega_3}\cos\Theta, \tag{11}$$

$$\frac{d\Phi}{d\tau} = \alpha^{-1/2}(\Omega_3 - \Omega_1 - \Omega_2), \tag{12}$$

$$\frac{d\Theta}{d\tau} = \alpha^{-1/2}(\omega_3 + \sqrt{\alpha}\tau - \Omega_3), \tag{13}$$

where we also introduced the rescaled amplitudes $B_j = A_j\sqrt{\Omega_j}$. We proceed to the analysis of the slow evolution of our system described by these equations next.

First, we assume that the terms with ε and η in Eqs. (10) and (11) are sufficiently small, so that $\Omega_j \approx \omega_j$. This is our *small nonlinear frequency shift* assumption. Then, taking square roots of (10) and (11) and linearizing to first order in ε and η, we obtain

$$\frac{dB_j}{d\tau} = -\lambda B_k B_3 \sin\Phi, \quad j,k=1,2, \quad j\neq k, \tag{14}$$

$$\frac{dB_3}{d\tau} = \lambda B_1 B_2 \sin\Phi - \mu\sin\Theta, \tag{15}$$

$$\frac{d\Theta}{d\tau} = \tau - \lambda\frac{B_1 B_2}{B_3}\cos\Phi - \frac{\mu}{B_3}\cos\Theta, \tag{16}$$

$$\frac{d\Phi}{d\tau} = \lambda\left(\frac{B_1 B_2}{B_3} - \frac{B_2 B_3}{B_1} - \frac{B_1 B_3}{B_2}\right)\cos\Phi + \frac{\mu}{B_3}\cos\Theta. \tag{17}$$

Here $\lambda = \varepsilon/(4\sqrt{\omega_2\omega_3\alpha})$ and $\mu = \eta/(2\sqrt{\omega_3\alpha})$ are the reduced coupling parameter and driving amplitude, respectively. We shall consider the effect of violation of the small nonlinear frequency shift assumption in Sec. V. Finally, by defining the phase shifts $\varphi_j = \psi_j - \omega_j t$ such that $\dot{\varphi}_j = \Omega_j - \omega_j \ll 1$, and introducing slow complex amplitudes $b_j(\tau) = B_j(\tau)e^{-i\varphi_j(\tau)}$, we rewrite Eqs. (14)–(17) in the compact form

$$\frac{db_j}{d\tau} = -i\lambda b_k^* b_3, \quad j,k=1,2, \quad j\neq k, \tag{18}$$

$$\frac{db_3}{d\tau} = -i\lambda b_1 b_2 - i\mu e^{-i\tau^2/2}. \tag{19}$$

This system describes the initial evolution stage in our driven system, including the process of capture into resonance.

B. Linear evolution stages

The process of capture of our system into resonance with the drive can be divided into different evolution stages. In the initial, linear evolution stage, we neglect the right-hand side (RHS) in (18) for $j=1$, assuming $|b_2|, |b_3| \ll |b_1|$. This yields $b_1 = b_{10} = 1$. The equations for the remaining two oscillators in this stage become

$$\frac{db_2}{d\tau} + i\lambda b_3 = 0, \tag{20}$$

$$\frac{db_3}{d\tau} + i\lambda b_2 = -i\mu e^{-i\tau^2/2}, \tag{21}$$

subject to zero initial conditions, $b_{2,3}(\tau_0) = 0$. This inhomogeneous system of equations can be solved by the method of undetermined coefficients, yielding the result

$$b_2(\tau) = c_+(\tau)e^{i\lambda\tau} + c_-(\tau)e^{-i\lambda\tau}, \tag{22}$$

$$b_3(\tau) = -c_+(\tau)e^{i\lambda\tau} + c_-(\tau)e^{-i\lambda\tau}, \tag{23}$$

where

$$c_\pm = \pm i\frac{\mu}{2}\int_{\tau_0}^{\tau} e^{-i(\tau'^2/2 \pm \lambda\tau')}d\tau' = \pm i\frac{\mu}{\sqrt{2}}e^{i\lambda^2/2} I, \tag{24}$$

$I = \int_a^b e^{-iu^2}du$, and $a = (\tau_0 \pm \lambda)/\sqrt{2}$, $b = (\tau \pm \lambda)/\sqrt{2}$. We can also express I as

$$I = \sqrt{\frac{\pi}{2}}\{[C(a') - C(b')] - i[S(a') - S(b')]\}, \tag{25}$$

where C and S are Fresnel integrals [15] evaluated at $a' = -\sqrt{2/\pi}a$ and $b' = -\sqrt{2/\pi}b$. Alternatively, one can use Fresnel auxiliary functions f and g to write

$$I = i\sqrt{\frac{\pi}{2}}[\, e^{-ia^2}(f+ig)|_{a'} - \, e^{-ib^2}(f+ig)|_{b'}]. \tag{26}$$

Next, we seek an asymptotic approximation for I at $|a|, |b| \gg 1$. Assuming some large negative initial τ_0, such that $a' \gg 1$, we consider two possibilities, (i) $b \gg 1$ and (ii) $b < 0$, $|b| \gg 1$, separately. In case (i) we use the symmetry relations $C(-x) = -C(x)$, $S(-x) = -S(x)$ and the asymptotic values $C(x) \to 1/2$, $S(x) \to 1/2$ at $x \to \infty$ in Eq. (25) to approximate

$$I = \sqrt{\frac{\pi}{2}}(1-i). \tag{27}$$

In case (ii) for $x \gg 1$, $f(x) \sim 1/\pi x$ and $g(x) \sim 1/\pi^2 x^3$. Therefore, by neglecting g in Eq. (26), we obtain

$$I = i\frac{1}{2}\left(\frac{e^{-ib^2}}{b} - \frac{e^{-ia^2}}{a}\right). \tag{28}$$

Now, we use (27) and (28) in the expressions for $c_{\pm}$, and write solutions $b_{2,3}$ [see Eqs. (22) and (23)]. We distinguish between two different stages of initial evolution in our system. In stage (a), $\tau<0$, $|\tau| \gg \lambda$, we have

$$b_2(\tau) = \mu e^{-i\tau^2/2}\left(\frac{e^{i(\tau^2-\tau_0^2)/2}}{\tau_0^2-\lambda^2}P + \frac{\lambda}{\tau^2-\lambda^2}\right), \tag{29}$$

$$b_3(\tau) = \mu e^{-i\tau^2/2}\left(\frac{e^{i(\tau^2-\tau_0^2)/2}}{\tau_0^2-\lambda^2}Q + \frac{\tau}{\tau^2-\lambda^2}\right), \tag{30}$$

where $P=-\lambda\cos[\lambda(\tau-\tau_0)]+i\tau_0\sin[\lambda(\tau-\tau_0)]$ and $Q=-\tau_0\cos[\lambda(\tau-\tau_0)]+i\lambda\sin[\lambda(\tau-\tau_0)]$. For continuing phase locking between the third oscillator and the drive, the τ dependence of phase φ_3 of b_3 should be approximately $\tau^2/2$. Then the expression in the parentheses in Eq. (30) must be nearly real, which is the case when

$$\frac{\sqrt{\tau_0^2+\lambda^2}}{\tau_0^2-\lambda^2} \ll \frac{|\tau|}{\tau^2-\lambda^2}. \tag{31}$$

For negative times τ, the last inequality is satisfied if $\lambda \ll |\tau| \ll |\tau_0|$. Therefore, taking $|\tau_0|$ large enough guarantees capture of the third oscillator into resonance (resulting in a bounded phase mismatch $\Theta=\psi_d-\psi_3$) at some $|\tau|=|\tau_\Theta| \gg \lambda$. Since the value of the dominant term in the parentheses in Eq. (30) in this case is negative, the phase mismatch assumes the value $\Theta=\pi$ after capture into resonance. Next, assuming phase locking of the third oscillator and the drive, we discuss the initial evolution of the phase mismatch $\Phi \equiv \psi_3-\psi_1-\psi_2 \approx \varphi_3-\varphi_2$ between the three oscillators. When phase locked, the τ dependence of phase φ_2 should be the same as that of phase φ_3, i.e., $\varphi_2 \sim \tau^2/2$. This is the case when the expression in the parentheses in Eq. (29) is approximately real, i.e., for

$$\frac{\sqrt{\tau_0^2+\lambda^2}}{\tau_0^2-\lambda^2} \ll \frac{\lambda}{\tau^2-\lambda^2}. \tag{32}$$

At large negative times τ and τ_0, this inequality is satisfied for $\lambda \ll |\tau| \ll \sqrt{\lambda|\tau_0|}$, guaranteeing phase locking of the three oscillators (boundness of Φ) at some $|\tau|=|\tau_\Phi| \gg \lambda$. Since the value of the dominant term in the parentheses in Eq. (29) is positive, while the value of the dominant term in the parentheses of (30) is negative, the phase mismatch Φ is locked at π.

In the second stage [stage (b)] of initial evolution, $|\tau| \ll \lambda$, and

$$b_2(\tau) = \mu\frac{1+i}{2}\sqrt{\pi}e^{i\lambda^2/2+i\lambda\tau} - \frac{\mu}{2}Q', \tag{33}$$

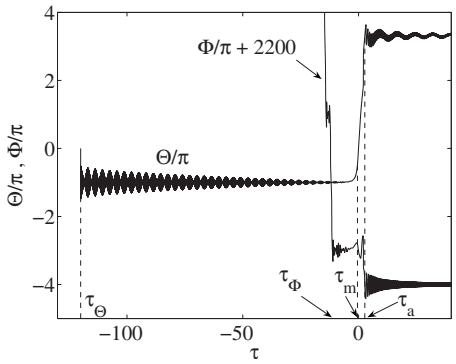

FIG. 3. Evolution of phase mismatches Θ and Φ ($\lambda=1, \mu=1.8$).

$$b_3(\tau) = -\mu\frac{1+i}{2}\sqrt{\pi}e^{i\lambda^2/2+i\lambda\tau} - \frac{\mu}{2}P', \tag{34}$$

where $Q'=e^{-i\tau_0^2/2-i\lambda(\tau_0-\tau)}/(\tau_0-\lambda)-e^{-i\tau^2/2}/(\tau-\lambda)$ and $P'=e^{-i\tau_0^2/2-i\lambda(\tau_0-\tau)}/(\tau_0-\lambda)-e^{-i\tau^2/2}/(\tau-\lambda)$. The first terms in Eqs. (33) and (34) are dominant for $|\tau_0-\lambda| \gg 1$ and $|\tau-\lambda| \gg 1$. Therefore, $b_2(\tau) \approx -b_3(\tau)$ and the phase mismatch Φ locks at π. At the same time, the phase locking between the third oscillator and the drive discontinues, and the phase mismatch Θ varies rapidly in time. We present a numerical example of different stages of initial evolution of the system in Fig. 3. The times $\tau_\Theta=-120$ and $\tau_\Phi=-11.3$ at which Θ and Φ become locked, as well as the escape of Θ from resonance at $\tau=\tau_m=-0.5$, are seen in the figure.

C. Asymptotic autoresonant quasi-steady-state

We have found numerically that for a range of parameters λ and μ the system is recaptured into resonance at a specific time $\tau=\tau_a>0$ ($\tau_a=2.7$ in the example shown in Fig. 3), beyond which the phase mismatches Φ and Θ perform converging oscillations around the values

$$\Phi_s \approx 0 \pmod{2\pi}, \quad \Theta_s \approx \text{const} \pmod{2\pi}. \tag{35}$$

We shall discuss this problem of recapture into resonance in Sec. IV, while, in this section, we focus on the evolution of the system after the recapture. Consequently, we analyze the system (14)–(17) under assumptions (35) at $\tau>\tau_a$. The left-hand sides of Eqs. (16) and (17) can then be replaced by 0, so, approximating $\cos\Phi \approx 1$, one can write

$$\tau - \lambda\frac{B_1B_2}{B_3} - \frac{\mu\cos\Theta_s}{B_3} = 0, \tag{36}$$

$$\lambda\left(\frac{B_1B_2}{B_3} - \frac{B_2B_3}{B_1} - \frac{B_1B_3}{B_2}\right) + \frac{\mu\cos\Theta_s}{B_3} = 0. \tag{37}$$

We supplement the last two equations by the Manley-Rowe relation

$$B_1^2 - B_2^2 = B_{10}^2 - B_{20}^2 = 1, \tag{38}$$

obtained from Eqs. (14). Thus, we have a system of three algebraic equations for B_1, B_2, and B_3. We seek asymptotic

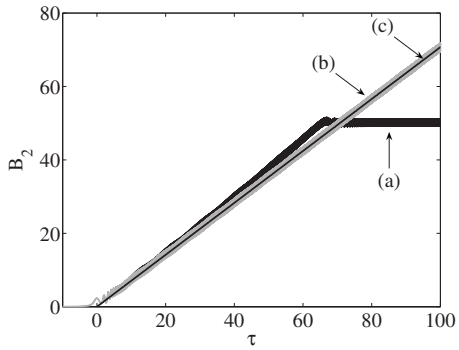

FIG. 4. Comparison of amplitude B_2 versus time in different approximations. (a) The numerical solution of the adiabatic equations (3)–(7), (b) the small nonlinear frequency shift limit, Eqs. (14)–(17), and (c) the asymptotic limit (39).

solution of this system at large positive τ, such that the amplitudes B_j are sufficiently large and one can neglect the terms $\mu \cos \Theta_s/B_3$ in Eqs. (36) and (37). This asymptotic quasi-steady-state can be easily found:

$$B_{1s} = B_{2s} = \frac{\tau}{\sqrt{2}\lambda}, \tag{39}$$

$$B_{3s} = \frac{\tau}{2\lambda}. \tag{40}$$

We illustrate these result in Fig. 4, showing the numerical solution of the adiabatic set of equations (3)–(7) [line (a)], the solution of Eqs. (14)–(17) for small nonlinear frequency shifts [line (b)], and the asymptotic result (39) [line (c)]. The calculations were performed for the same parameters $\varepsilon = 0.031$ and $\eta = 0.0197$ (i.e., $\lambda = 1$ and $\mu = 1.8$). One observes a good agreement between the adiabatic solution (a) and the small nonlinear frequency shift model (b) for $\tau < 70$. However, when nonlinear frequency shifts become large the escape from resonance at $\tau = 70$ is observed. This phenomenon will be discussed later, in Sec. V. One can also see in the figure a good agreement between the adiabatic solution (b) and its asymptotic limit (c) for $\tau > 10$.

III. STABILITY OF THE ASYMPTOTIC QUASI-STEADY-STATE

At this stage, we proceed to study stability of the autoresonant quasi-steady-state derived above. The evolution of deviations of phase mismatches $\delta\Theta = \Theta - \langle\Theta\rangle$, $\delta\Phi = \Phi - \langle\Phi\rangle$, from the values $\langle\Theta\rangle$ and $\langle\Phi\rangle$ averaged over integration time in the numerical example with $\lambda = 1$, $\mu = 10$ is plotted in Fig. 5. The black regions in the figure include high-frequency, visually unresolved oscillations of $\delta\Theta$ and $\delta\Phi$, while the boundaries of the black regions represent the envelopes of these high-frequency oscillations. One can also see that high-frequency oscillations of $\delta\Theta$ are superimposed on a low-frequency oscillating component and that maxima of $|\delta\Theta|$ and $|\delta\Phi|$ decrease in time, indicating stability of the quasi-steady-state. Further information about these oscillations is revealed by calculating the Fourier spectra of $\delta\Theta$ and

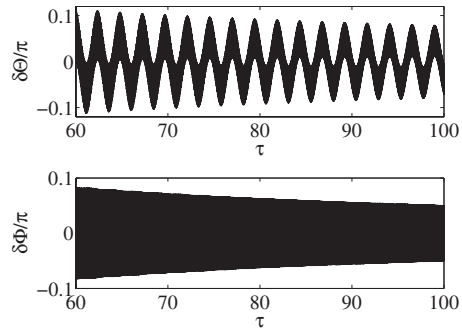

FIG. 5. Evolution of the phase mismatch deviations $\delta\Theta$ and $\delta\Phi$ from the quasi-steady-state. The boundaries of the black regions represent envelopes of visually unresolved high-frequency oscillations.

$\delta\Phi$ (see Fig. 6). One can see that, indeed, the spectrum of $\delta\Theta$ has two components: (a) a narrowband at low frequency around some Ω_1' and (b) a wideband, higher-frequency component between Ω_2' and Ω_2'' with a decreasing spectral density at higher frequencies. The spectrum of $\delta\Phi$ is similar to that of $\delta\Theta$, but has only the wideband component and a higher spectral density compared to that in $\delta\Theta$. The analysis of the evolution equations for $\delta\Theta$ and $\delta\Phi$ is presented next, aiming at explaining the features of their Fourier spectra.

A. Linear stability analysis

We proceed by allowing small deviations from the quasi-steady-state solution,

$$B_j = B_{js} + \delta B_j, \quad \Phi = \Phi_s + \delta\Phi, \quad \Theta = \Theta_s + \delta\Theta. \tag{41}$$

Then, linearizing in (14)–(17), and assuming, for simplicity, that $\lambda\mu \gg 1.5$, i.e. (see Sec. IV), $\Theta_s \approx \pi$, we obtain

$$\frac{d(\delta B_j)}{d\tau} = -\lambda B_{ks} B_{3s} \delta\Phi, \quad j,k = 1,2, \quad j \neq k, \tag{42}$$

$$\frac{d(\delta B_3)}{d\tau} = \lambda B_{1s} B_{2s} \delta\Phi + \mu \delta\Theta, \tag{43}$$

$$\frac{d(\delta\Theta)}{d\tau} = \frac{\tau \delta B_3 - \lambda(B_{1s}\delta B_2 + B_{2s}\delta B_1)}{B_{3s}}, \tag{44}$$

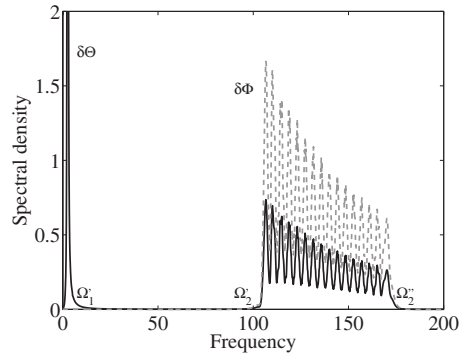

FIG. 6. Fourier spectra of phase mismatch deviations shown in Fig. 5, $\delta\Theta$ (solid line) and $\delta\Phi$ (dashed line).

$$\frac{d(\delta\Phi)}{d\tau} = \sqrt{2}\lambda(\delta B_1 + \delta B_2 - 2\sqrt{2}\delta B_3). \tag{45}$$

The differentiation of (45) with respect to τ and the use of Eqs. (42) and (43) yields

$$\frac{d^2(\delta\Phi)}{d\tau^2} = -3\tau^2\delta\Phi - 4\lambda\mu\delta\Theta. \tag{46}$$

Similarly, by substituting Eqs. (39) and (40) into Eq. (44), differentiating the result with respect to τ, and using Eqs. (42) and (43), we obtain,

$$\frac{d^2(\delta\Theta)}{d\tau^2} = 2\tau^2\delta\Phi + 2\lambda\mu\delta\Theta. \tag{47}$$

The last two coupled, second-order linear equations comprise a set for studying stability of the asymptotic quasi-steady-state in our system. We shall analyze this set below by using a WKB-type analysis involving singular value decomposition of the associated matrix problem [16].

First, we write Eqs. (46) and (47) in matrix form

$$\frac{d^2}{d\tau^2}\mathbf{X} + \mathbf{M}\cdot\mathbf{X} = 0, \tag{48}$$

where $\mathbf{X}=(\delta\Phi,\delta\Theta)^T$ and

$$\mathbf{M} = \begin{pmatrix} 3\tau^2 & 4\lambda\mu \\ -2\tau^2 & -2\lambda\mu \end{pmatrix}.$$

Next, we represent $\mathbf{X}$ as

$$\mathbf{X} = \mathrm{Re}(\mathbf{Y}e^{i\Psi}), \tag{49}$$

where the real amplitude vector $\mathbf{Y}$ is assumed to be slow [such that $d\mathbf{Y}/d\tau$ is of $O(\delta)$, δ being a small dimensionless parameter describing this slowness of variation in the system], while the eikonal phase Ψ is fast, but, nevertheless, the frequency $\tilde{\Omega}=d\Psi/d\tau$ is slow. Then, substituting Eq. (49) into Eq. (48) and neglecting the second derivative of $\mathbf{Y}$, we arrive at

$$i\left(2\tilde{\Omega}\frac{d\mathbf{Y}}{d\tau} + \frac{d\tilde{\Omega}}{d\tau}\mathbf{Y}\right) + \mathbf{D}\cdot\mathbf{Y} = 0, \tag{50}$$

where

$$\mathbf{D} = \mathbf{M} - \tilde{\Omega}^2\mathbf{I} = \begin{pmatrix} 3\tau^2 - \tilde{\Omega}^2 & 4\lambda\mu \\ -2\tau^2 & -2\lambda\mu - \tilde{\Omega}^2 \end{pmatrix}, \tag{51}$$

while $\mathbf{I}$ is a unit matrix. Now, by observing that $d\mathbf{Y}/d\tau$, $d\tilde{\Omega}/d\tau$ in Eq. (50) are of $O(\delta)$, we seek solutions of this equation in the form of the series $\mathbf{Y}=\mathbf{Y}_0+\mathbf{Y}_1+\cdots$, where the terms $\mathbf{Y}_n$ are viewed as $O(\delta^n)$. Then, in zero order, Eq. (50) yields $\mathbf{D}\cdot\mathbf{Y}_0=\mathbf{0}$, requiring $|\mathbf{D}|=0$, yielding the characteristic frequencies

$$\tilde{\Omega}_{1,2} = \sqrt{\frac{2\lambda\mu - 3\tau^2}{2}\left(-1 \pm \sqrt{1 - \frac{8\lambda\mu\tau^2}{(2\lambda\mu - 3\tau^2)^2}}\right)}. \tag{52}$$

Asymptotically, at $\tau\to\infty$,

$$\tilde{\Omega}_1 \to \sqrt{\frac{2}{3}\lambda\mu}, \quad \tilde{\Omega}_2 \to \sqrt{3}\tau. \tag{53}$$

Next, in seeking $\mathbf{Y}_0$, we go to first order in Eq. (50), i.e.,

$$\mathbf{D}\cdot\mathbf{Y}_1 + i\left(2\tilde{\Omega}\frac{d\mathbf{Y}_0}{d\tau} + \frac{d\tilde{\Omega}}{d\tau}\mathbf{Y}_0\right) = 0. \tag{54}$$

In dealing with this equation, we perform singular value decomposition of $\mathbf{D}$ [16],

$$\mathbf{D} = d_1\mathbf{v}_1\mathbf{u}_1^H + d_2\mathbf{v}_2\mathbf{u}_2^H, \tag{55}$$

where, generally, complex pairs of vectors $\mathbf{u}_1$, $\mathbf{u}_2$ and $\mathbf{v}_1$, $\mathbf{v}_2$ are orthonormal ($\mathbf{u}_j^H\cdot\mathbf{u}_k=\delta_{jk}$, $\mathbf{v}_j^H\cdot\mathbf{v}_k=\delta_{jk}$), d_j ($j=1,2$) are real singular values of $\mathbf{D}$, while the superscript H denotes the transpose complex conjugate. We decompose $\mathbf{Y}_0=y_1\mathbf{u}_1+y_2\mathbf{u}_2$, so that in zero order ($\mathbf{D}\cdot\mathbf{Y}_0=0$)

$$d_1y_1 = 0, \quad d_2y_2 = 0. \tag{56}$$

Then, by choosing $d_1=0$ and $d_2\neq 0$, we have $y_2=0$ and $\mathbf{Y}_0=y_1\mathbf{u}_1$, as well as

$$\mathbf{D}\cdot\mathbf{u}_1 = d_1\mathbf{v}_1 = 0, \quad \mathbf{v}_1^H\cdot\mathbf{D} = d_1\mathbf{u}_1^H = 0. \tag{57}$$

Then, we multiply the first-order Eq. (54) by $\mathbf{v}_1^H$ from the left and use (57) to get the slow equation for y_1:

$$\tilde{\Omega}\mathbf{v}_1^H\cdot\mathbf{u}_1\frac{dy_1}{d\tau} + \left(\tilde{\Omega}\mathbf{v}_1^H\cdot\frac{d\mathbf{u}_1}{d\tau} + \frac{1}{2}\frac{d\tilde{\Omega}}{d\tau}\mathbf{v}_1^H\cdot\mathbf{u}_1\right)y_1 = 0. \tag{58}$$

Here, we use the asymptotic forms of $\mathbf{D}$ evaluated at $\tilde{\Omega}_{1,2}$, i.e.,

$$\mathbf{D} = \begin{pmatrix} 3\tau^2 & 0 \\ -2\tau^2 & 0 \end{pmatrix}, \quad \mathbf{D} = \begin{pmatrix} 0 & 0 \\ -2\tau^2 & -3\tau^2 \end{pmatrix}, \tag{59}$$

in calculating $\mathbf{u}_1$ and $\mathbf{v}_1^H$, respectively. The final result of this calculation yields the asymptotic dependence of $\mathbf{Y}_0=y_1\mathbf{u}_1$ on time, which, after returning to our original variables $\delta\Phi$ and $\delta\Theta$, yields $(\delta\Phi,\delta\Theta)^T=\mathbf{X}_1+\mathbf{X}_2$, where the two modes of oscillations are

$$\mathbf{X}_1 = \mathrm{Re}\left[\begin{pmatrix} 0 \\ 1 \end{pmatrix} z_1 \exp\left(i\int\tilde{\Omega}_1(\tau')d\tau'\right)\right] \tag{60}$$

and

$$\mathbf{X}_2 = \mathrm{Re}\left[\begin{pmatrix} 3/\sqrt{13} \\ -2/\sqrt{13} \end{pmatrix}\frac{z_2}{\sqrt{\tau}}\exp\left(i\int\tilde{\Omega}_2(\tau')d\tau'\right)\right]. \tag{61}$$

Here the constant coefficients $z_{1,2}$ and the initial phases in the exponents are determined by the initial conditions on X and $dX/d\tau$. Thus, small deviations of the phase mismatches from the quasi-steady-state values (35) do not increase with τ, i.e., the state is stable for all values of λ and μ. Furthermore, now we can explain all the features of the Fourier spectra of $\delta\Phi$ and $\delta\Theta$, illustrated in Fig. 6. Indeed, the narrow low-frequency band of the spectrum of $\delta\Theta$ at frequency Ω_1' is associated with the $\tilde{\Omega}_1$ term in Eqs. (60) and (61), which vanishes for $\delta\Phi$. In the numerical example in Fig. 6, $\lambda=1$ and $\mu=10$, having $\tilde{\Omega}_1\approx\sqrt{\frac{2}{3}\lambda\mu}=2.6$. The wideband, higher-

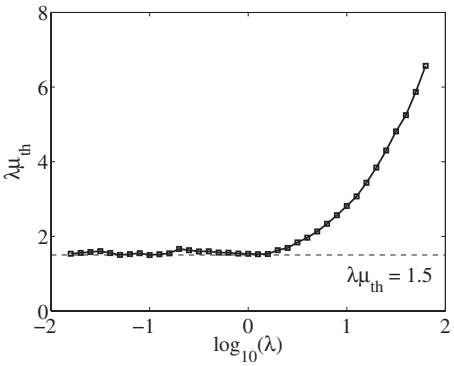

FIG. 7. Autoresonance threshold μ_{th} vs the coupling parameter λ.

frequency spectrum component between Ω_2' and Ω_2'' can be associated with the $\tilde{\Omega}_2$ term. Since the spectra were computed in the time interval $60 \le \tau \le 100$, $\Omega_2' \approx \tilde{\Omega}_2|_{\tau=60} = 60\sqrt{3} \approx 104$ and $\Omega_2'' \approx \tilde{\Omega}_2|_{\tau=100} \approx 100\sqrt{3} \approx 173$. The decrease of the spectral density for higher frequencies is explained by the $1/\sqrt{\tau}$ dependence in $\mathbf{X}_2$. The ratio between the spectral density of the high-frequency contributions in $\delta\Phi$ and $\delta\Theta$ is approximately $(3/2)^2 = 2.25$, which is the square of the ratio between the magnitudes of the $\tilde{\Omega}_2$ terms in the expressions for $\delta\Phi$ and $\delta\Theta$. All these results are in full agreement with our numerical spectra.

IV. THE THRESHOLD PHENOMENON

This section discusses the threshold phenomenon with respect to the driving amplitude for capturing our system into resonance and the conditions for continuing autoresonance in the system. Recall that our driven system evolves subject to initial amplitudes $B_{10}=1$, and $B_{20,30}=0$. We have shown in Sec. II B that the system is captured into resonance at $\Theta \approx \pi$, $\Phi \approx \pi$ in the linear evolution stage under these initial conditions, regardless of the initial phase of the oscillators or their phase relative to that of the drive. Therefore, the dynamics of the system in later stages is determined by the parameters λ and μ only. In particular, the successful capture of the system into autoresonance, resulting in a quasi-steady-state, depends on the values of these parameters. Our numerical scan of the (λ, μ) parameter space revealed that for successful autoresonance at a specific value of the coupling parameter λ, the driving parameter μ must be larger than some threshold value μ_{th}. The numerical results for the product $\lambda\mu_{th}$ versus λ are shown in Fig. 7. One can see that for weaker couplings, $\lambda < 2$, $\lambda\mu_{th} \approx 1.5$. In contrast, for $\lambda > 2$, the value of $\lambda\mu_{th}$ increases monotonically with λ. Now, we take the sum of Eq. (14) for $j=1$ and 2, and express $\sin\Phi$ in terms of B_j

$$\sin\Phi = -\frac{B_1 dB_1/d\tau + B_2 dB_2/d\tau}{2\lambda B_1 B_2 B_3}. \tag{62}$$

The substitution of this expression into (15) yields $\sin\Theta$ in terms of B_j:

$$\sin\Theta = -\frac{1}{2\mu B_3}\left(2B_3\frac{dB_3}{d\tau} + B_1\frac{dB_1}{d\tau} + B_2\frac{dB_2}{d\tau}\right). \tag{63}$$

This expression, assuming the quasi-steady-state, yields $\sin\Theta_s = -1.5/\lambda\mu$. Requiring $\sin\Theta_s \ge -1$, we find the necessary condition, $\lambda\mu \ge 1.5$, for the existence of the quasi-steady-state. Indeed, our numerical results in Fig. 7 illustrate satisfaction of this condition when in autoresonance. We also see that, for weaker couplings, $\lambda < 2$, this condition is not only necessary, but sufficient for continuing autoresonance in the system.

V. VALIDITY OF THE SMALL NONLINEAR FREQUENCY SHIFT MODEL

It has been observed in Sec. II C that, in contrast to the prediction of the small nonlinear shift model (14)–(17), the full adiabatic evolution equations (3)–(7) predict escape from autoresonance at large τ. To deal with this issue, we have extended our asymptotic quasi-steady-state of Eqs. (8) and (10)–(13) to second order in τ, under the assumption $d\Phi/d\tau = d\Theta/d\tau = 0$ and neglecting the last term in (11). The resulting expressions for B_j and Ω_j are

$$B_{1,2} = a_1\tau + a_2\tau^2, \quad B_3 = a_3\tau + a_4\tau^2, \tag{64}$$

where $a_1 = 2\sqrt{2\omega_1\omega_2\omega_3\alpha}/\varepsilon$, $a_2 = \sqrt{2}(4\omega_1\omega_2 + 3\omega_1\omega_3 + 3\omega_2\omega_3)\alpha/8\varepsilon\sqrt{\omega_1\omega_2\omega_3}$, $a_3 = 2\sqrt{\omega_1\omega_2\omega_3\alpha}/\varepsilon$, $a_4 = (4\omega_1\omega_2 + \omega_1\omega_3 + \omega_2\omega_3)\alpha/4\varepsilon\sqrt{\omega_1\omega_2\omega_3}$, and

$$\Omega_j = \omega_j + \frac{1}{2}\sqrt{\alpha}\tau + \frac{\alpha(\omega_k - \omega_j)}{16\omega_j\omega_k}\tau^2, \quad j,k = 1,2, \quad j \ne k, \tag{65}$$

$$\Omega_3 = \omega_3 + \sqrt{\alpha}\tau. \tag{66}$$

Note that, to $O(\tau)$, Eqs. (64) are the same as in the asymptotic small nonlinear frequency shift limit (39), (40). The positive $O(\tau^2)$ term in (64) explains the deviation of the numerical solution of the full set of adiabatic equations (3)–(7) from the linear quasi-steady-state solution (39) for $\tau < 70$ as shown in Fig. 4. Next, we eliminate $\sin\Theta$ from (8) and (9), yielding

$$\sin\Theta = -\frac{\sqrt{\alpha\Omega_3}}{\eta B_3}\left(2B_3\frac{dB_3}{d\tau} + B_1\frac{dB_1}{d\tau} + B_2\frac{dB_2}{d\tau}\right). \tag{67}$$

Then, assuming that the system is in a quasi-steady-state, substituting expressions (64) and (66), and demanding $\sin\Theta \ge -1$, one obtains a τ-dependent inequality for the system parameters. This inequality can be satisfied for times τ less than a critical time τ_e, beyond which the quasi-steady-state ceases to exist. This escape time can be estimated by taking $O(\tau)$ term in the Taylor expansion of the RHS in (67), yielding

$$\tau_e \approx \frac{\frac{2}{3}\varepsilon\eta\sqrt{\omega_1\omega_2} - 8\omega_3\alpha}{\alpha^{3/2}(8\omega_1\omega_2 + 3\omega_3^2)}. \tag{68}$$

For example, for the set of parameters used in Fig. 2, one finds $\tau_e \approx 71$, in reasonably good agreement with $\tau_e = 67$ from

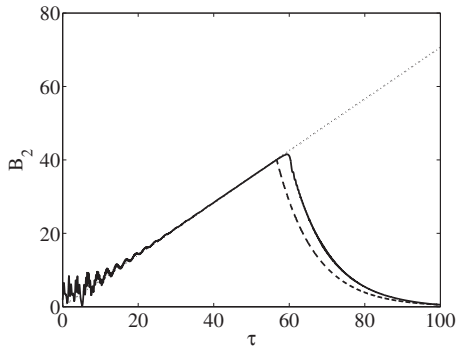

FIG. 8. Autoresonance in a dissipative system. The numerical solution of the adiabatic set (14), (16), (17), and (69) (solid line) is compared to that given by Eq. (71) (dashed line). The dotted line represents the asymptotic solution (39).

the numerical solution of the full adiabatic set of equations (3)–(7) and $\tau_e=50$ from the original set of equations (1) and (2). Finally, we observe that τ_e increases with increase of the driving amplitude, allowing the system to reach higher excitation levels.

VI. ADDITIONAL EFFECTS

A. Dissipation

Here we discuss the influence of a dissipation term of form $-\beta\dot{x}_3$ on the RHS of Eq. (2). Addition of this term in our adiabatic analysis results in a set of equations identical to (14), (16), and (17), but (15) is replaced by

$$\frac{dB_3}{d\tau} = \lambda B_1 B_2 \sin\Phi - \mu \sin\Theta - \nu B_3, \tag{69}$$

where $\nu=\beta/(2\sqrt{\alpha})$. Then, similarly to the developments in Sec. IV, one obtains the following necessary condition for existence of the autoresonant quasi-steady-state:

$$\lambda\mu \geq \frac{3}{2} + \frac{\nu}{2}\tau. \tag{70}$$

Therefore, in the case of a dissipative system, the autoresonant threshold value of $\lambda\mu$ increases with τ and, for given λ and μ, the quasi-steady-state exists for $\tau \leq \tau_d$ only, where $\tau_d=(2\lambda\mu-3)/\nu$. For later times, the system escapes from resonance, and the oscillator amplitudes decay exponentially,

$$B_j(\tau) = B_{js}(\tau_d) e^{-(\nu/3)(\tau-\tau_D)}, \tag{71}$$

where B_{js} are given by (39) and (40). We present an example of such evolution of a dissipative system in Fig. 8. The numerical solution of the slow system (14), (16), (17), and (69) (solid line) in the figure is compared to that given by Eq. (71) (dashed line). The parameters were $\lambda=1$, $\mu=10$, and $\nu=0.3$. The dotted line represents the asymptotic autoresonant asymptotic solution (39). One can see that adding dissipation in the system contributes to the convergence of B_2 to the asymptotic solution. The predicted value of τ_d and the evolution of B_2 for $\tau > \tau_d$ are similar to the solution of the slow evolution equations in our system.

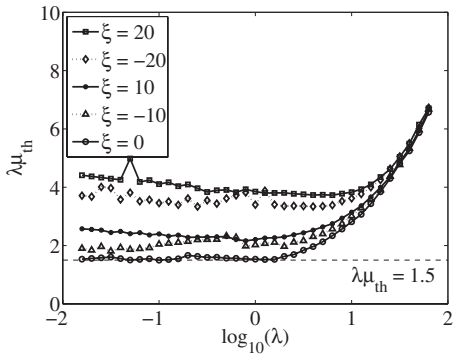

FIG. 9. Autoresonance threshold at different values of the linear frequency mismatch parameter ξ.

B. Frequency mismatch

Here we discuss the effect of a mismatch between the linear frequencies of the decoupled oscillators. We write $\omega_1+\omega_2=\omega_3+\Delta\omega$ where $\Delta\omega$ may be either positive or negative. In this case, similarly to the developments in Sec. II A, one obtains a set of equations identical to (14)–(16), but Eq. (17) is replaced by

$$\frac{d\Phi}{d\tau} = \lambda\left(\frac{B_1B_2}{B_3} - \frac{B_2B_3}{B_1} - \frac{B_1B_3}{B_2}\right)\cos\Phi + \frac{\mu}{B_3}\cos\Theta + \xi, \tag{72}$$

where $\xi=\Delta\omega/\sqrt{\alpha}$. We have used this system for numerical investigation of the threshold for autoresonance in the presence of linear frequency mismatch. The threshold μ_{th} in the driving amplitude was defined as the minimal value of μ for which the system was captured into the autoresonant state. Figure 9 presents the numerical results for $\lambda\mu_{th}$ versus λ. The case $\xi=0$ corresponds to our previous results (see Sec. IV) for a perfect linear frequency matching. For cases with $\xi\neq 0$, the dominant effects are the increase of $\lambda\mu_{th}$ with $|\xi|$ and the weak dependence on the sign of ξ.

VII. CONCLUSIONS

(a) We have demonstrated efficient control of resonant three-oscillator interactions by using an additional, external, chirped frequency forcing applied to one of the oscillators. In analyzing this phenomenon, we have divided the evolution of the driven R3OI system into several stages, each characterized by a different type of resonant interaction, and applied the adiabatic approximation in studying the driven phase-locked evolution of the system.

(b) A simple quasi-steady-state of the driven R3OI system, where the slow amplitudes of the interacting oscillators increase in proportion to the deviation of the driving frequency from the linear resonance, was found and analyzed. The quasi-steady-state stage discontinues at a certain time τ_e and the energy of the driven system saturates. By increasing the driving amplitude η, one extends the duration of the autoresonant state, allowing excitation to higher energy.

(c) We have shown that, for weak excitations, when the nonlinear frequency shifts due to the interaction between the

oscillators are small, the quasi-steady-state is characterized by a double phase locking, where the phase mismatches $\Phi = \psi_3 - \psi_2 - \psi_1$ between the interacting oscillators and $\Theta = \psi_d - \psi_3$ between the drive and the driven (third) oscillator are locked at $\Phi \approx 0$ and $\Theta \approx$ const. We have also shown that this double phase locking is linearly stable.

(d) We have studied the threshold μ_{th} in the amplitude of the drive for successful excitation of the autoresonant state. We have shown that the product $\lambda\mu$ of the coupling and driving parameters in the system must exceed 3/2 to have the asymptotic autoresonant quasi-steady-state. We have seen numerically that, for a sufficiently weak coupling, $\lambda < 2$, μ_{th} satisfies the relation $\lambda\mu_{th} \approx 1.5$. For stronger couplings, $\lambda\mu_{th} > 1.5$.

(e) The addition of dissipation causes the escape from autoresonance at some time τ_d, for which we have an estimate. Beyond τ_d the slow amplitudes decay exponentially with time.

(f) Finally, we have studied numerically the effect of linear frequencies mismatch $\Delta\omega = \omega_3 - \omega_2 - \omega_1$ on the autoresonance in our system. We have observed that the product $\lambda\mu_{th}$ is a monotonically increasing function of $|\Delta\omega|$.

(g) It seems interesting to extend the present theory to resonant three-wave interactions and generalize it to more than one space and time dimension.

ACKNOWLEDGMENTS

This work was supported by the U.S.-Israel Binational Science Foundation (Grant No. 2004033).

[1] R. Z. Sagdeev and A. A. Galeev, *Nonlinear Plasma Theory* (W. A. Benjamin, Ney York, 1969).
[2] W. L. Kruer, *The Physics of Laser Plasma Interactions*, reprint ed. (Westview Press, Boulder, CO, 2001).
[3] A. Yariv, *Quantum Electronics*, 3rd ed. (John Wiley, New York, 1989).
[4] K. Trulsen and C. C. Mei, J. Fluid Mech. **290**, 345 (1995).
[5] A. P. Mayer, Phys. Rep. **256**, 237 (1995).
[6] A. Rieman, Rev. Mod. Phys. **51**, 311 (1979).
[7] V. N. Oraevskii, V. P. Pavlenko, H. Wilhelmsson, and E. Ya. Kogan, Phys. Rev. Lett. **30**, 49 (1973).
[8] L. Friedland, Phys. Rev. Lett. **69**, 1749 (1992).
[9] S. Yariv and L. Friedland, Phys. Rev. E **48**, 3072 (1993).
[10] E. A. Williams, B. I. Cohen, L. Divol, M. R. Dorr, J. A. Hittinger, D. E. Hinkel, A. B. Langdon, R. K. Kirkwood, D. H. Froula, and S. H. Glenzer, Phys. Plasmas **11**, 231 (2004).
[11] L. Friedland and A. G. Shagalov, Phys. Rev. E **71**, 036206 (2005).
[12] Computer code MATLAB ver. 7 (The Math Works Inc., Natick, 2004).
[13] L. Cohen, *Time Frequency Analysis* (Prentice-Hall, Englewood Cliffs, NJ, 1994).
[14] J. Fajans and L. Friedland, Am. J. Phys. **69**, 1096 (2001).
[15] *Handbook of Mathematical Functions*, Natl. Bur. Stand. Appl. Math. Ser. No. 55, edited by M. Abramovitz and I. A. Stegun (U.S. GPO, Washington, D.C., 1968).
[16] B. Noble, *Applied Linear Algebra* (Prentice-Hall, Englewood Cliffs, NJ, 1969), pp. 335–338.